Ceramics International xxx (xxxx) xxx

Contents lists available at ScienceDirect

Ceramics International

journal homepage: www.elsevier.com/locate/ceramint

Sc- and W-substitution and tuning of phase transition in the $Al_2Mo_3O_{12}$

Zhiping Zhang [a], Yuenan Wang [b], Hongfei Liu [b,*], Wei Wang [b]

[a] Department of Mechanical and Electrical Engineering, Guangling College, Yangzhou University, Yangzhou, 225000, PR China
[b] School of Physical Science and Technology, Yangzhou University, Yangzhou, 225002, PR China

ARTICLE INFO

Keywords:
Phase transition
Negative thermal expansion
Chemical substitution
Solid-state reaction

ABSTRACT

$Al_2Mo_3O_{12}$ is a typical negative thermal expansion (NTE) material, whose thermal expansion behavior depends on its crystal phase. The thermal shock caused by temperature-induced phase transition limits its wide application. The two series of $Al_{2-x}Sc_xMo_3O_{12}$ ($0 \leq x \leq 1$) and $Al_2Mo_{3-x}W_xO_{12}$ ($0 \leq x \leq 2.5$) solid solutions with controllable phase transition temperature were synthesized via single cation substitution at the A or B position. The problem of thermal shock caused by the change of temperature is effectively solved in the synthesized $Al_{1.6}Sc_{0.4}Mo_3O_{12}$ and $Al_2Mo_{0.5}W_{2.5}O_{12}$, showing stable NTE performance above room temperature, and the coefficients of thermal expansion of which are -2.19×10^{-6} °C^{-1} in 100–550 °C and -4.25×10^{-6} °C^{-1} in 85–500 °C, respectively. A-site cation substitution is a more effective way to tune the thermal expansion properties of $Al_2Mo_3O_{12}$, which is attributed to the fact that the bond strength of A-O is weaker than that of B–O in the compound.

1. Introduction

With the rapid development of precision manufacturing and testing technology, there is an ever-growing demand for low thermal expansion materials that are not easily influenced by the change of temperature. The discovery of negative thermal expansion (NTE) materials offers an effective way to manufacture low thermal expansion materials through controlling the coefficients of thermal expansion (CTEs) of materials. In the past two decades, NTE materials have developed rapidly and become a new branch of material research [1–5]. The new type of NTE materials $A_2B_3O_{12}$ (A is a trivalent main group metal, transition metal, and lanthanide metal; B is W and Mo) have excellent NTE performance and chemical flexibility [6–10]. $Al_2Mo_3O_{12}$ is of great interest for application, which can be used to synthesize materials with low or even zero CTE, such as $Sc_{0.7}Al_{0.3}Mo_3O_{12}$, and $Al_2Mo_3O_{12}$/PE materials [11,12]. Furthermore, $Al_2Mo_3O_{12}$ is considered to be promising for application in modern microwave communications, due to its low dielectric constant [13,14]. However, $Al_2Mo_3O_{12}$ experiences a structural change at 200 °C during the heating process, and the thermal shock affected by the change of temperature limits its practical use in the application [15,16]. It has become significant work to shift the phase transition temperature of $Al_2Mo_3O_{12}$ from high temperature to room temperature.

When the A-site cation of $A_2B_3O_{12}$ is occupied by Sc, Al, In, Cr, and Fe five elements, the corresponding tungstates and molybdates are isomorphic. Ari M reported that there was a decrease in the phase transition temperature of $Cr_{2x}Fe_{2-2x}Mo_3O_{12}$, $Al_{2x}Cr_{2-2x}Mo_3O_{12}$ and $Al_{2x}Fe_{2-2x}Mo_3O_{12}$ compounds with the increase of low electronegativity A_{2x} content [17]. Our earlier work also proved that the low electronegativity Sc^{3+} substitution can decrease the phase transition temperature of $Al_2Mo_3O_{12}$ [18]. The phase transition temperatures of Sc-substituted $AlScMo_3O_{12}$, $Al_{1.7}Sc_{0.3}W_3O_{12}$, $In_{0.5}Sc_{1.5}Mo_3O_{12}$, $In_{1.1}Sc_{0.9}W_3O_{12}$ and $Sc_{0.5}Cr_{1.5}Mo_3O_{12}$ are generally lower than that of unsubstituted $Al_2Mo_3O_{12}$, $Al_2W_3O_{12}$ $In_2Mo_3O_{12}$, $In_2W_3O_{12}$ and $Cr_2Mo_3O_{12}$, respectively, ascribing to the lowest electronegativity of scandium among these five elements [19–23]. On the contrary, the phase transition temperature of $Sc_{0.8}Fe_{1.2}Mo_3O_{12}$ is higher than that of unsubstituted $Sc_2Mo_3O_{12}$ [24]. The reported researches show that chemical substitution of scandium at the A position is considered to be one of the promising approaches to inhibit the high phase transition temperature of $Al_2Mo_3O_{12}$. However, few studies have previously been carried out on the substitution at the B position in $A_2B_3O_{12}$ compounds except the $Al_2Mo_{3-x}W_xO_{12}$ series [25,26]. Partial substitution of W by Mo has some effects on the structural and thermal expansion properties of $Al_2W_3O_{12}$. Furthermore, the phase transition temperature of $Al_2W_3O_{12}$ (−6 °C) is lower than that of $Al_2Mo_3O_{12}$ (200 °C) [27]. It is possible to tune the phase transition of $Al_2Mo_3O_{12}$ through cation substitution at the B position, and tungsten is chosen as the substituted cation.

* Corresponding author. School of Physical Science and Technology, Yangzhou University, Yangzhou 225002, PR China.
E-mail addresses: liuhf@yzu.edu.cn, zp-hf@163.com (H. Liu).

https://doi.org/10.1016/j.ceramint.2021.04.127
Received 6 February 2021; Received in revised form 24 March 2021; Accepted 14 April 2021
Available online 16 April 2021

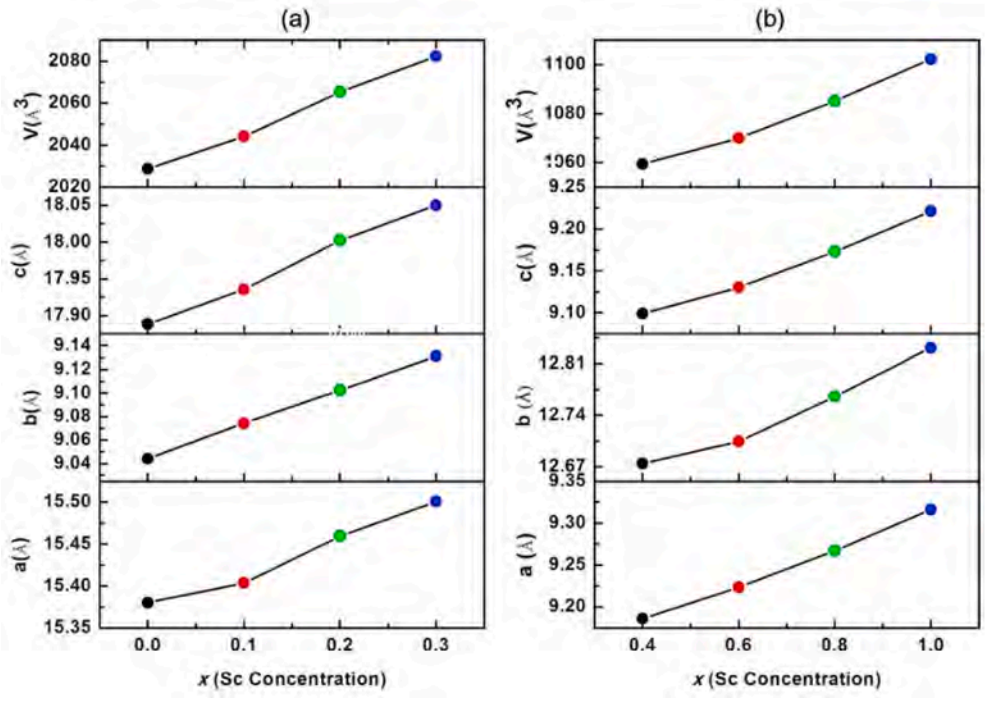

Fig. 1. (a) XRD patterns of synthesized $Al_{2-x}Sc_xMo_3O_{12}$ ($0 \leq x \leq 1$) solid solutions and (b) Partial XRD patterns of $Al_{2-x}Sc_xMo_3O_{12}$ solid solutions in the 2θ range of 12.5–30°

Table 1
Lattice parameters and crystal structure in $Al_{2-x}Sc_xMo_3O_{12}$ solid solutions.

Sc^{3+}-content **(x)**	a/Å	b/Å	c/Å	V/Å^3	Crystal structure
0	15.3803	9.0443	17.8880	2028.73	Monoclinic
0.1	15.4036	9.0743	17.9354	2044.02	
0.2	15.4595	9.1025	18.0020	2065.26	
0.3	15.5007	9.1311	18.0501	2082.29	
0.4	9.1862	12.6743	9.0990	1059.40	Orthorhombic
0.6	9.2237	12.7042	9.1304	1069.85	
0.8	9.2670	12.7655	9.1730	1085.14	
1.0	9.3161	12.8312	9.2231	1102.28	

This present investigation aimed to tune the phase transition temperature of $Al_2Mo_3O_{12}$ by single cation substitution at the A or B site. The effects of Sc- and W- substitution on tuning of phase transition of $Al_2Mo_3O_{12}$ will be compared. The effects and mechanism of Sc substitution for Al as well as W substitution for Mo on the crystal structure, morphology, phase transition temperature, and NTE performance of $Al_2Mo_3O_{12}$ were also studied.

2. Experimental

The series of $Al_{2-x}Sc_xMo_3O_{12}$ ($0 \leq x \leq 1$) and $Al_2Mo_{3-x}W_xO_{12}$ ($0 \leq x \leq 2.5$) samples were prepared using solid-state reaction. Stoichiometric amounts of Al_2O_3(99.95%), Sc_2O_3(99.95%), MoO_3(99.95%) and WO_3 (99.95%) were ball milled in alcoholic medium for 12 h. The resulting mixtures were dried, pre-calcined at 600 °C, and then uniaxially pressed into 10 mm diameter bar-shaped pellets. Finally, the resulting pellets were sintered at 780 °C, and held there for 12 h. The twice-sintering process at 900 °C was used for $Al_2Mo_{3-x}W_xO_{12}$ ($0 \leq x \leq 2.5$) samples to achieve the complete reaction of the reactants.

X-ray diffraction (XRD) was done on a Shimadzu XRD-7000 (CuKα radiation) with a scan range of 10–60°. Microstructures and elemental mapping were analyzed using scanning transmission electron microscope (STEM, FEI Tecnai F30 S-TWIN) and energy dispersive X-ray spectrometer (EDX). X-ray photoelectron spectroscopy (XPS) was recorded by an ESCALAB 250Xi system. Morphology of the samples was characterized using a scanning electron microscope (SEM, TESCAN VEEGA3). Moreover, the thermal expansion measurements were performed on thermomechanical analyzer (TMA, Seiko 6300). The heating rate is 10 °C·min^{-1} in 25–600 °C. Differential scanning calorimetry (PerkinElmer DSC-8500) was also used to analyze the phase transition process of the samples, and the heating rate is 5 °C·min^{-1} in 25–350 °C.

3. Results and discussion

3.1. Analysis of the $Al_{2-x}Sc_xMo_3O_{12}$ solid solutions

Fig. 1a shows the phase evolution of $Al_2Mo_3O_{12}$ solid solutions substituted with Sc. For the samples with substituted Sc-content $x \leq 0.3$, there are no noticeable changes in the XRD patterns of $Al_{2-x}Sc_xMo_3O_{12}$, and crystallize in the $Al_2Mo_3O_{12}$-type monoclinic structure. When the

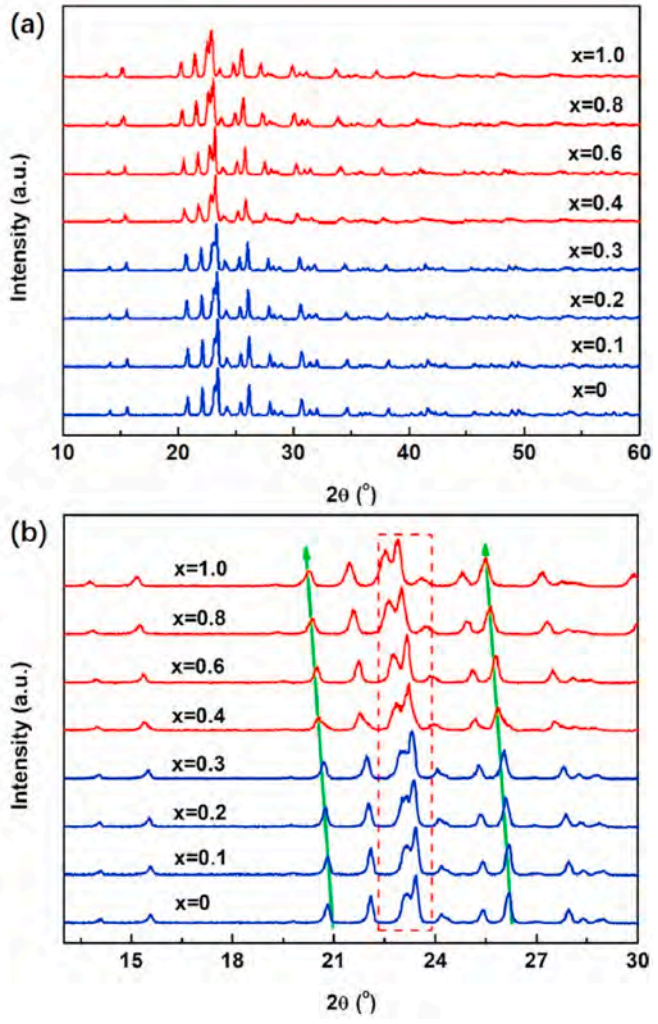

Fig. 2. Compositional dependence of the lattice parameters and volume in $Al_{2-x}Sc_xMo_3O_{12}$ (a) $0 < x \leq 0.3$ and (b) $0.4 \leq x \leq 1$.

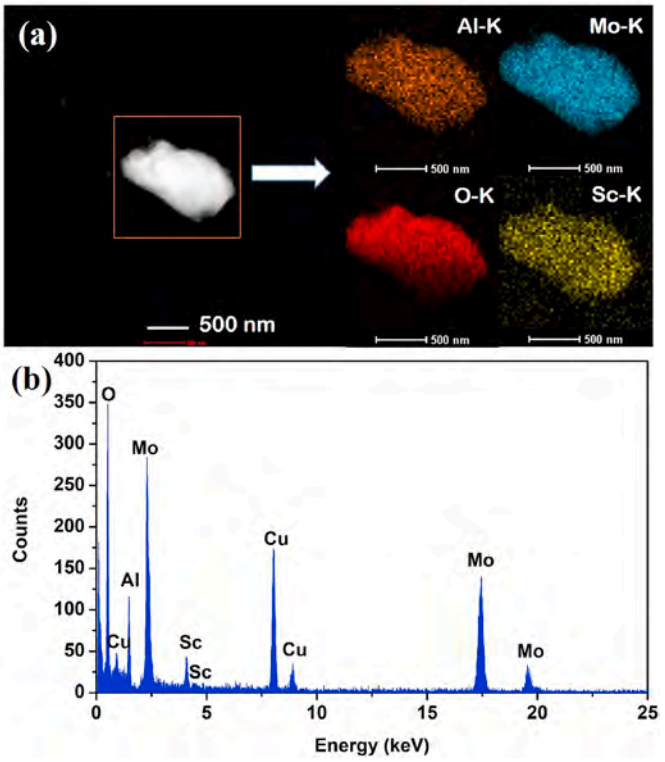

Fig. 3. (a) Elemental mapping and (b) EDX spectrum of $Al_{1.6}Sc_{0.4}Mo_3O_{12}$ powder.

Sc-content is further increased to $0.4 \leq x \leq 1$, all the XRD patterns of $Al_{2-x}Sc_xMo_3O_{12}$ samples still appear to single-phase with minimal change in the presence of a sharp diffraction peak at $2\theta = 22.5–24°$, as shown in Fig. 1b. Besides, the expanded diffraction peaks in the 12.5–30° 2θ range significantly shift towards lower angles as substituted Sc-content (x) increases, suggesting the expansion of lattice parameters.

The lattice parameters and crystal structure of $Al_{2-x}Sc_xMo_3O_{12}$ solid solutions, as calculated by Topas 5.0 software, are summarized in Table 1 and presented in Fig. 2. The crystal structure of $Al_{2-x}Sc_xMo_3O_{12}$ transforms from monoclinic ($x \leq 0.3$) into orthorhombic ($0.4 \leq x \leq 1$) symmetry with increasing Sc-content (x). The results indicate that a small amount (20%) of scandium substitution of $Al_2Mo_3O_{12}$ forms an orthorhombic phase with *Pnca* space group. For monoclinic and orthorhombic $Al_{2-x}Sc_xMo_3O_{12}$, the lattice parameters as well as volume increase nearly linearly with increasing x value, following Vegard's law (shown in Fig. 2).

Fig. 3a shows the elemental mapping images of the $Al_{1.6}Sc_{0.4}Mo_3O_{12}$ sample. It can be seen that the main elements of Al, Sc, Mo, and O are uniformly distributed, revealing the fabrication of a homogeneous scandium dispersion in $Al_{1.6}Sc_{0.4}Mo_3O_{12}$. Fig. 3b shows the EDX spectrum of $Al_{1.6}Sc_{0.4}Mo_3O_{12}$ sample, indicating that the sample consists of four elements of Al, Sc, Mo and O. Cu is originated from the testing. According to the above XRD and STEM analysis, the high purity $Al_{1.6}Sc_{0.4}Mo_3O_{12}$ solid solution with single-phase is successfully prepared.

Fig. 4 depicts SEM images of $Al_{2-x}Sc_xMo_3O_{12}(0 \leq x \leq 0.6)$solid solutions with different Sc-content (x). All of the SEM images exhibit similar morphology with sphere-like grain. For $x = 0$, $Al_2Mo_3O_{12}$ shows a homogeneous structure with an average grain size ranging between 2 and 5 μm, as shown in Fig. 4a. When Sc-content increased from $x = 0.1$ to 0.3, the grain size of $Al_{2-x}Sc_xMo_3O_{12}$ becomes smaller and distributes more uniformly, however, the density of all samples does not improve significantly (Fig. 4b–d). For the samples with $0.4 \leq x \leq 0.6$, it is observed a relative decrease in the density of $Al_{2-x}Sc_xMo_3O_{12}$ samples, which is linked to the change of crystal structure (Fig. 4e and f).

Fig. 5 shows the thermal expansion curves of $Al_{2-x}Sc_xMo_3O_{12}$ solid solutions measured by TMA. Most curves exhibit fluctuations apparently in 30–550 °C due to the monoclinic-orthorhombic phase transition. The partial substitution of Sc for Al has a notable effect on the temperature-induced phase transition of $Al_{2-x}Sc_xMo_3O_{12}$. For the unsubstituted sample, the onset of the phase transition occurs at 191.2 °C (Fig. 5a). With increasing Sc content, the phase transition temperature of $Al_{2-x}Sc_xMo_3O_{12}$ shifts toward the lower temperature, and the NTE response temperature range is broadened, as illustrated in Fig. 5b–d and Table 2. As for samples with $x \geq 0.4$, no fluctuations are observed in the thermal expansion curves throughout the testing temperature range, indicating

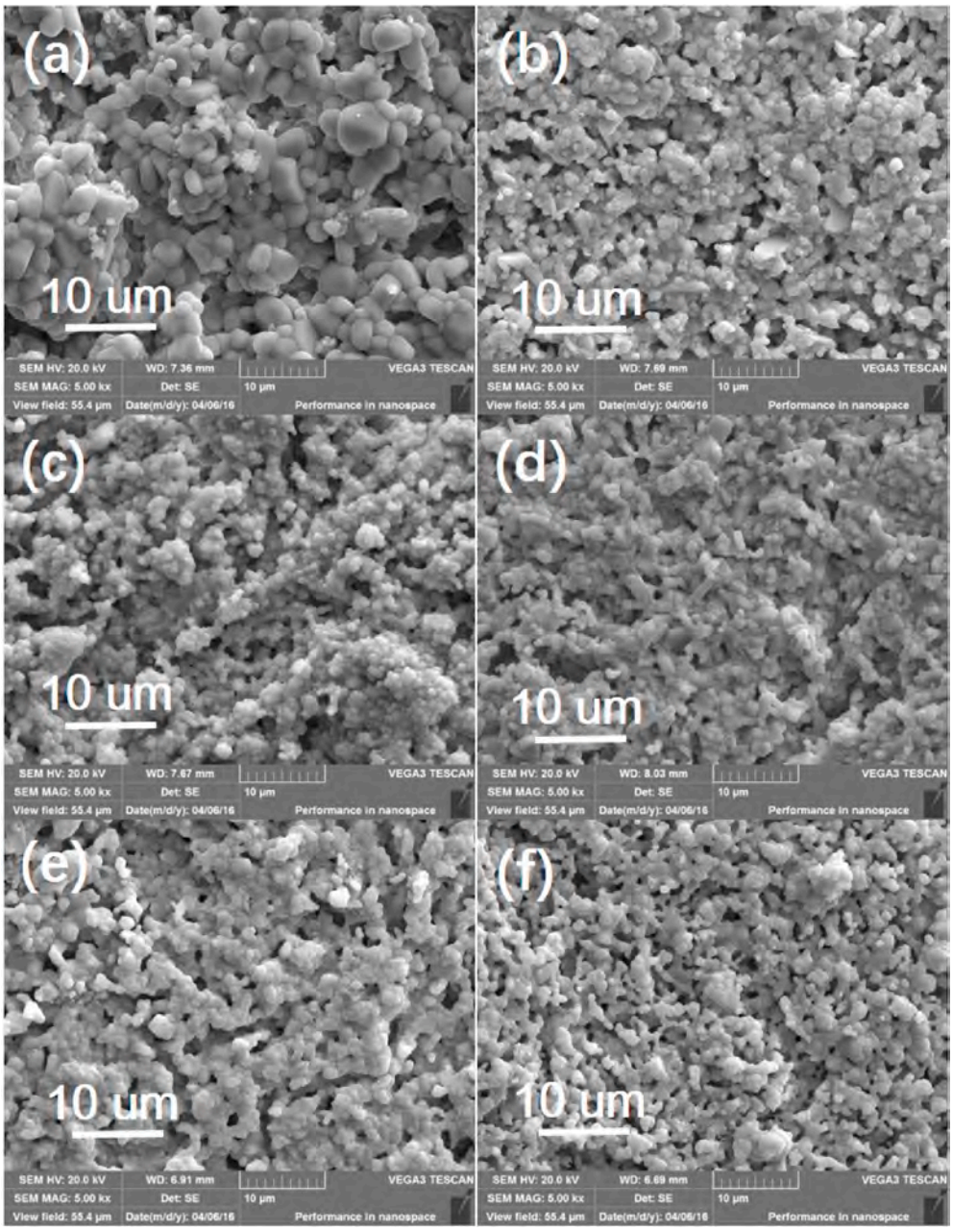

Fig. 4. Cross-sectional SEM images of $Al_{2-x}Sc_xMo_3O_{12}$ solid solutions sintered at 780 °C for 6 h (a) x = 0; (b) x = 0.1; (c) x = 0.2; (d) x = 0.3; (e) x = 0.4 and (f) x = 0.6.

the high phase transition temperature of $Al_2Mo_3O_{12}$ has shifted to room temperature and below, which means it can be used as NTE material from room temperature to decomposition temperature (Fig. 5e–h).

DSC was also carried out to study the phase transition process of $Al_{2-x}Sc_xMo_3O_{12}$ solid solutions. The variation of heat flow as a function of temperature for $Al_{2-x}Sc_xMo_3O_{12}$ ($0 \leq x \leq 0.4$) is plotted in Fig. 6. There is an endo peak in the curve due to the phase transition from lower symmetry monoclinic phase to higher symmetry orthorhombic phase. With increasing Sc content, the phase transition temperature of $Al_{2-x}Sc_xMo_3O_{12}$ ($0 \leq x \leq 0.4$) solid solutions presents a general decrease trend and drops from 204 °C to 74 °C, which are consistent with the TMA results (as shown in Table 3). The variation of the phase transition temperature with composition is found to obey the following equation $y = -439x + 205.6$, where y is the phase transition temperature, and x is the substituted Sc-content.

3.2. Analysis of the $Al_2Mo_{3-x}W_xO_{12}$ solid solutions

The XRD diffraction patterns of as-synthesized $Al_2Mo_{3-x}W_xO_{12}$ are presented in Fig. 7. $Al_2Mo_{3-x}W_xO_{12}$ solid solutions with x = 0, 0.5, 1, and 1.5 are single-phase, while the x = 2 and 2.5 samples show the traces of WO_3 impurity (Fig. 7b), which could be an indication that $Al_2Mo_{3-x}W_xO_{12}$ solid solutions with high purity were not formed at 780 °C. All members of $Al_2Mo_{3-x}W_xO_{12}$ ($0 \leq x \leq 2.5$) solid solutions crystallize in a monoclinic symmetry (space group $P2_1/a$).

To achieve the complete reaction of the reactants and enhance the

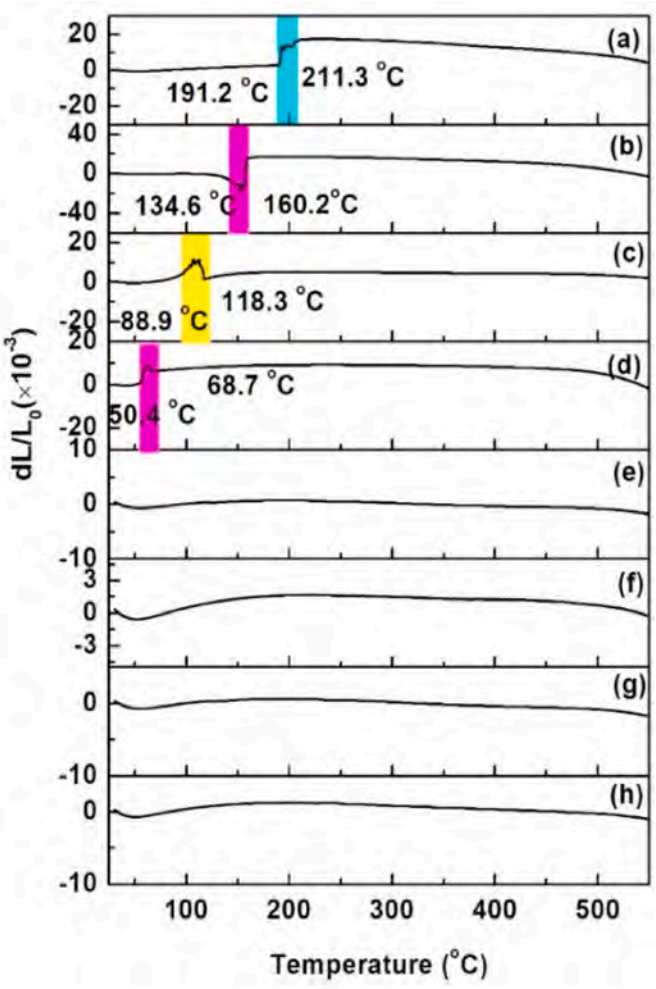

Fig. 5. Thermal expansion curves of $Al_{2-x}Sc_xMo_3O_{12}$ solid solutions (a) x = 0; (b) x = 0.1; (c) x = 0.2; (d) x = 0.3; (e) x = 0.4; (f) x = 0.6; (g) x = 0.8 and (h) x = 1.

purity of $Al_2Mo_{3-x}W_xO_{12}$, all the samples were secondary sintered at 900 °C. Fig. 8 illustrates the corresponding XRD patterns of the $Al_2Mo_{3-x}W_xO_{12}$. For pure $Al_2Mo_3O_{12}$, only the reflections characteristic for Al_2O_3 are detected due to the decomposition of the $Al_2Mo_3O_{12}$ at 900 °C. The XRD patterns reveal that $Al_2Mo_{3-x}W_xO_{12}$ phase evolves along the substituted tungsten-content (x). For the substituted samples with $x \leq 1.5$, no extra peak can be assigned to the impurity phase, and the XRD patterns can be indexed as the single-phase with $Al_2Mo_3O_{12}$-type monoclinic symmetry. For the x = 2 and 2.5 samples, the WO_3 completely reacted and form the $Al_2Mo_{3-x}W_xO_{12}$ solid solutions, which exhibit a well-crystallized single phase with $Al_2W_3O_{12}$-type orthorhombic symmetry. The difference between the monoclinic and orthorhombic structure is small, only the XRD peak at 2θ = 22.5–24° split into two distinct XRD peaks, which have been marked in Fig. 8. The above results also demonstrate that the increase of sintering temperature is beneficial for the complete reaction of raw materials for $x \geq 2$ and the formation of high purity products.

Fig. 9 depicts the TEM images and their corresponding EDX mapping image of the $Al_2MoW_2O_{12}$ sample. Fig. 10b and c displays lattice fringes with interplanar spacing of 3.84 Å, arising from the (112) planes, which reveals the well-defined lattice structure of orthorhombic $Al_2MoW_2O_{12}$. The EDX elemental mapping consists of Al, W, Mo, O, and Cu arising

Table 2
CTEs of $Al_{2-x}Sc_xMo_3O_{12}$ (x = 0, 0.1, 0.2, 0.3 and 0.4) solid solution.

Sample	CTEs ($\times 10^{-6}$ °C^{-1})	Testing temperature range (°C)	CTEs ($\times 10^{-6}$ °C^{-1})	Testing temperature range (°C)
$Al_2Mo_3O_{12}$	13.33	30–180	−16.17	230–550
$Al_{1.9}Sc_{0.1}Mo_3O_{12}$	0.65	30–120	−15.71	200–550
$Al_{1.8}Sc_{0.2}Mo_3O_{12}$	/	/	−2.69	200–550
$Al_{1.7}Sc_{0.3}Mo_3O_{12}$	/	/	−2.32	100–550
$Al_{1.6}Sc_{0.4}Mo_3O_{12}$	/	/	−2.19	100–550

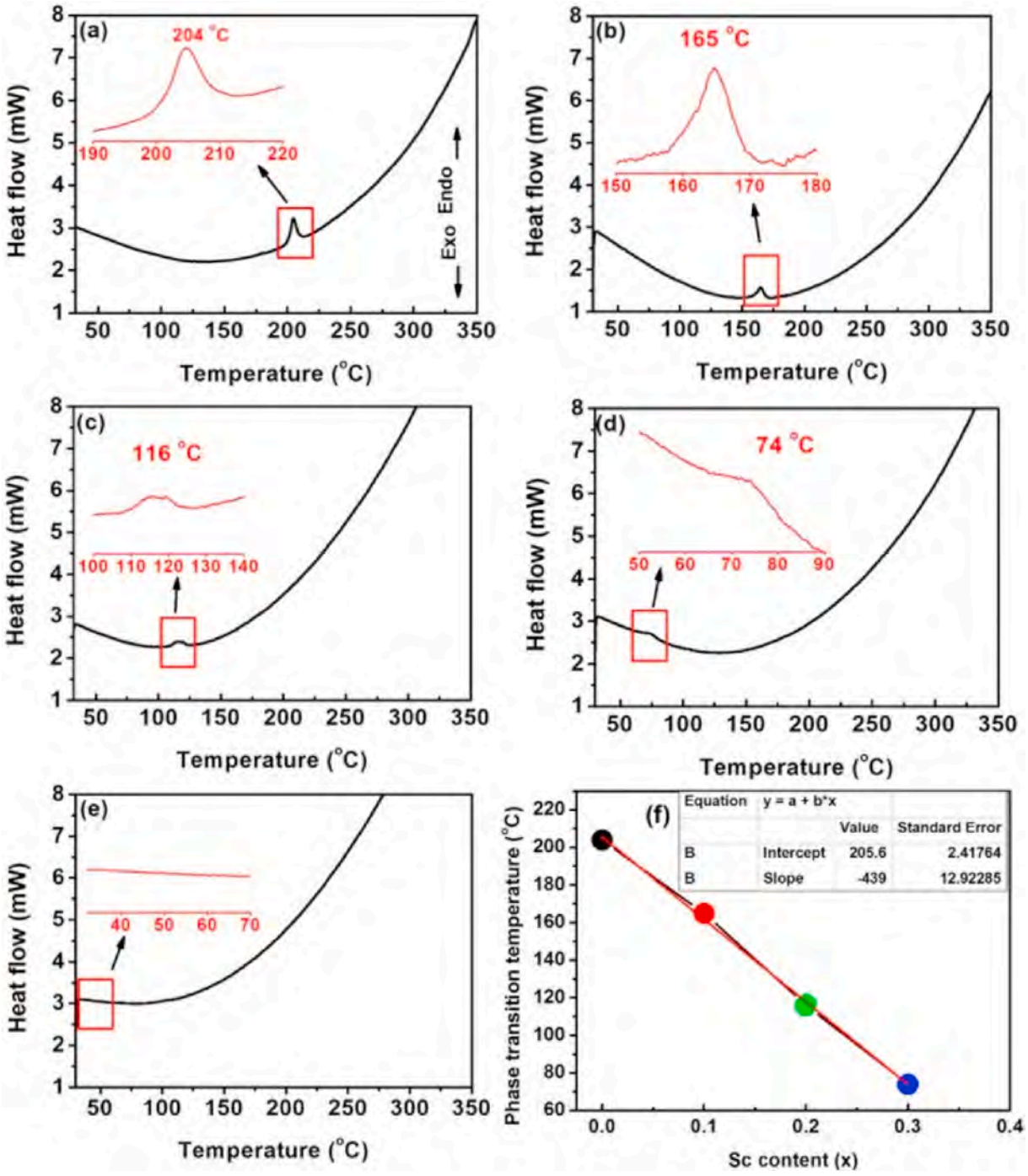

Fig. 6. The differential scanning calorimeter curves of $Al_{2-x}Sc_xMo_3O_{12}$ solid solutions (a) x = 0; (b) x = 0.1; (c) x = 0.2; (d) x = 0.3; (e) x = 0.4 and (f) the relationship between the phase transition and the content of Sc^{3+}-substitution.

Table 3
The phase transition temperature of $Al_{2-x}Sc_xMo_3O_{12}$ measured by DSC and TMA,respectively.

Samples	Phase transition temperature (°C)	
	measured by DSC	measured by TMA
$Al_2Mo_3O_{12}$	204	191.2–211.3
$Al_{1.9}Sc_{0.1}Mo_3O_{12}$	165	134.6–160.2
$Al_{1.8}Sc_{0.2}Mo_3O_{12}$	116	88.9–118.3
$Al_{1.7}Sc_{0.3}Mo_3O_{12}$	74	50.4–68.7
$Al_{1.6}Sc_{0.4}Mo_3O_{12}$	/	/

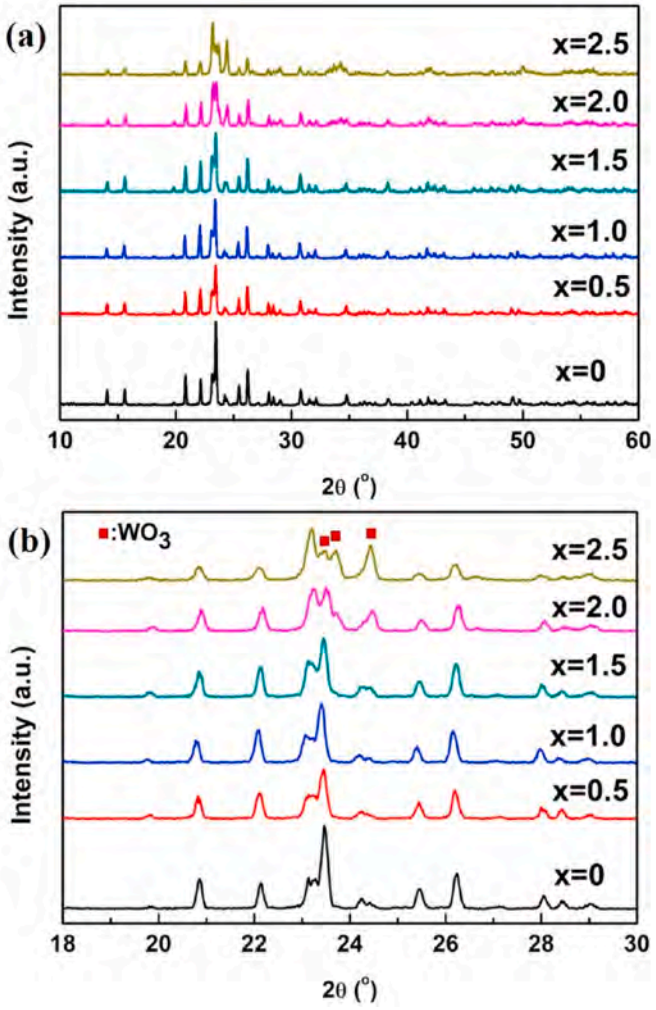

Fig. 7. XRD patterns of synthesized $Al_2Mo_{3-x}W_xO_{12}$ ($0 \leq x \leq 2.5$) solid solutions sintered at 780 °C in the 2θ range of (a)10–60°; (b) 18–30°

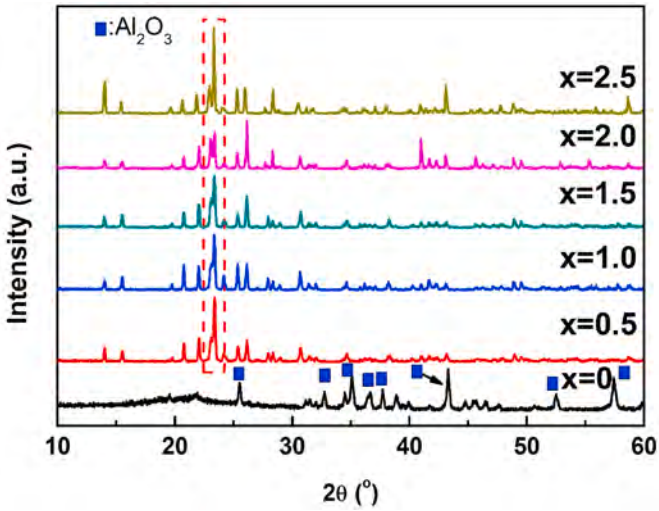

Fig. 8. XRD patterns of synthesized $Al_2Mo_{3-x}W_xO_{12}$ ($0 \leq x \leq 2.5$) solid solutions sintered at 900 °C.

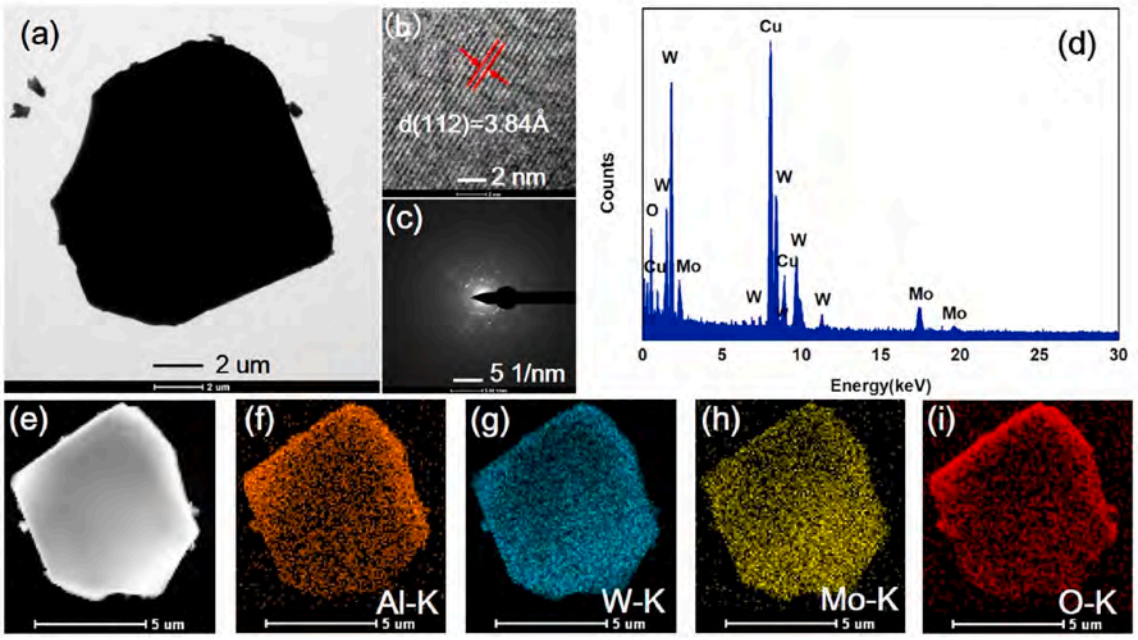

Fig. 9. (a) TEM image; (b) micro lattice fringe pattern; (c) selected area electron diffraction pattern; (d) EDX map for the TEM image of $Al_2MoW_2O_{12}$ powder; (e) STEM image and corresponding elements distribution of $Al_2MoW_2O_{12}$ particles (f) Al; (g) W; (h) Mo and (i) O.

from testing, revealing the purity of the sample (Fig. 9d). Elemental mapping on a single particle of $Al_2MoW_2O_{12}$ is provided in Fig. 10e-i, which further confirms that component elements (Al, W, Mo, and O) are homogeneously distributed throughout the investigated region. All the above results suggest successful preparation of single-phase $Al_2MoW_2O_{12}$ solid solution.

Fig. 10 depicts the wide-scan XPS spectrum of $Al_2MoW_2O_{12}$, and high-resolution spectra of Mo 3d and W 4f. It can be seen that the wide-scan spectrum of $Al_2MoW_2O_{12}$ consists of Al, W, Mo, and O, which is consistent with the EDX result. Mo 3d spectrum consists of two characteristic peaks of 232.8 eV and 236.0 eV, corresponding to Mo $3d_{5/2}$ and Mo $3d_{3/2}$, respectively, which stands for the existence of Mo (VI). The two distinctive peaks observed at 35.8 eV, 37.9 eV can be assigned to W $4f_{7/2}$ and W $4f_{5/2}$, respectively. The above XPS analysis confirms the coexistence of W^{6+} and Mo^{6+} in $Al_2MoW_2O_{12}$, indicating that Mo^{6+} can also be successfully substituted by W^{6+}.

The morphology has a significant influence on the thermal expansion performance test of ceramics, thus the microstructures of $Al_2Mo_{3-x}W_xO_{12}$ ($0 \le x \le 2.5$) ceramics were observed by scanning electron microscopy (SEM). Surface SEM images of $Al_2Mo_{3-x}W_xO_{12}$ samples are shown in Fig. 11. Based on the above XRD result, $Al_2Mo_3O_{12}$ decomposes after sintering at 900 °C. $Al_2Mo_3O_{12}$ sintered at 780 °C exhibits rod-like morphology and a relative loose microstructure (Fig. 11a). For the samples with $0.5 \le x \le 1.5$ sintered at 900 °C, it is evident that the crystal size of $Al_2Mo_{3-x}W_xO_{12}$ ceramics grows gradually, and the pores become less (Fig. 11b and c). Accordingly, the density of the $Al_2Mo_{3-x}W_xO_{12}$ ceramics is improved, which can be attributed to the high sintering temperature and increasing substitution of W. When $x \ge 2$, the microstructure of $Al_2Mo_{3-x}W_xO_{12}$ ceramics changed, some rod-like crystals are observed, which may caused by the crystal structure change, as shown in Fig. 11d and e. Additionally, the further increase of W-content (x) has no remarkable effects on the density of $Al_2Mo_{3-x}W_xO_{12}$ ceramics. These observations suggest that all the synthesized $Al_2Mo_{3-x}W_xO_{12}$ ($0 \le x \le 2.5$) samples have a denser microstructure.

The temperature dependence of thermal expansion curves for $Al_2Mo_{3-x}W_xO_{12}$ ceramics are depicted in Fig. 12. When $x \le 1.5$, a sudden change in all the thermal expansion curves of $Al_2Mo_{3-x}W_xO_{12}$ ceramics was observed, which was induced by the phase transition. As expected, this high temperature-induced phase transition is notably tuned by the tungstate substitution. As the increase of substituted W-content, the phase transition temperature of $Al_2Mo_{3-x}W_xO_{12}$ ($0 \le x \le 2.5$) samples decreases towards the lower temperature, and the NTE response temperature range is broaden monotonically. Note that the phase transition temperature of $Al_2Mo_{3-x}W_xO_{12}$ samples with $x \ge 2$ has been shifted to room temperature and below, exhibiting stable NTE performance throughout the whole testing temperature range, which suggests that the samples with these compositions overcome the defect of thermal shock caused by phase transition. Table 4 summarizes the CTEs of $Al_2Mo_{3-x}W_xO_{12}$ solid solutions measured by TMA. The magnitude of CTEs of $Al_2Mo_{3-x}W_xO_{12}$ ceramics gradually decreases with increasing W-content, which is ascribed to the CTE of parent phase orthorhombic $Al_2W_3O_{12}$($\alpha_l = 3 \times 10^{-6}$ °C^{-1}) [26] is lower than that of $Al_2Mo_3O_{12}$ ($\alpha_l = -18.06 \times 10^{-6}$ °C^{-1}). However, $Al_2Mo_{0.5}W_{2.5}O_{12}$ still exhibits NTE with a linear CTE of -4.25×10^{-6} °C^{-1} from 85 to 500 °C. In summary, the partial substitution of Mo by W successfully decreases the phase transition temperature and broadens the NTE response temperature range of $Al_2Mo_3O_{12}$.

In this work, tuning the phase transition temperature of $Al_2Mo_3O_{12}$ to room temperature and broadening its NTE response temperature range is achieved by single cation Sc^{3+}- or W^{6+}- substitution. The synthesized $Al_{1.6}Sc_{0.4}Mo_3O_{12}$ and $Al_2Mo_{0.5}W_{2.5}O_{12}$ solid solutions show stable NTE performance above room temperature. In comparison, the substitution rate of Sc at the A position is 20%, and 66.7% for W at the B position. The difference in the substituted content is due to the strength of the bond. The polyhedral frame structure of $Al_2Mo_3O_{12}$ is composed of MoO_4 tetrahedra and AlO_6 octahedra. It is ascribed to the fact that the Al–O bond belonging to the covalent bond in AlO_6 octahedra is weaker than that of the Mo–O bond in MoO_4 tetrahedra, which belongs to the ionic bond, ultimately, it is easier to tune the properties of $Al_2Mo_3O_{12}$ by A-site substitution. From the perspective of cation electronegativity, A-site substituted Sc is lower than that of Al, and the ability to attract electrons is weaker, which leads to the electron concentration around the O atom, resulting in the increase of O–O repulsion force. The O–O repulsion force drives the occurrence of phase transition of $Al_{2-x}Sc_xMo_3O_{12}$, resulting in lower phase transition temperature with increasing Sc-content.

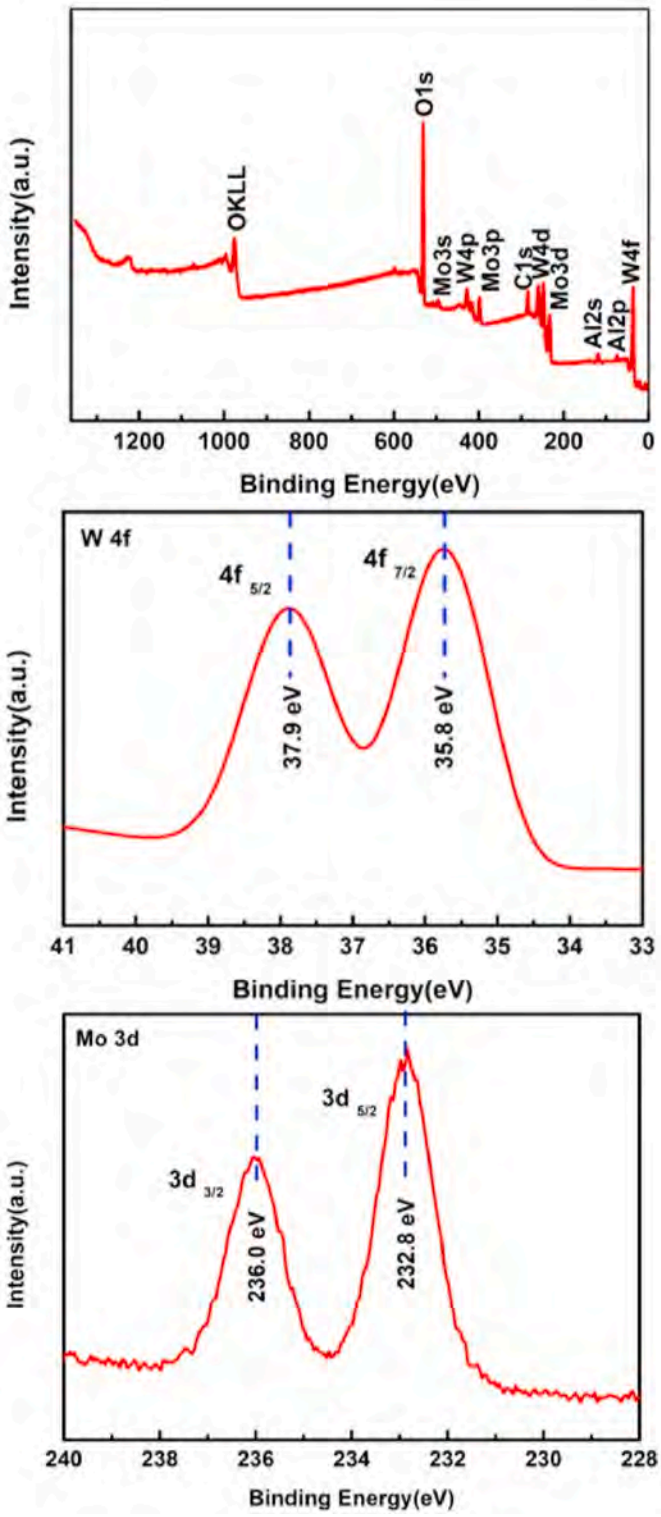

Fig. 10. XPS spectra for the synthesized $Al_2MoW_2O_{12}$.

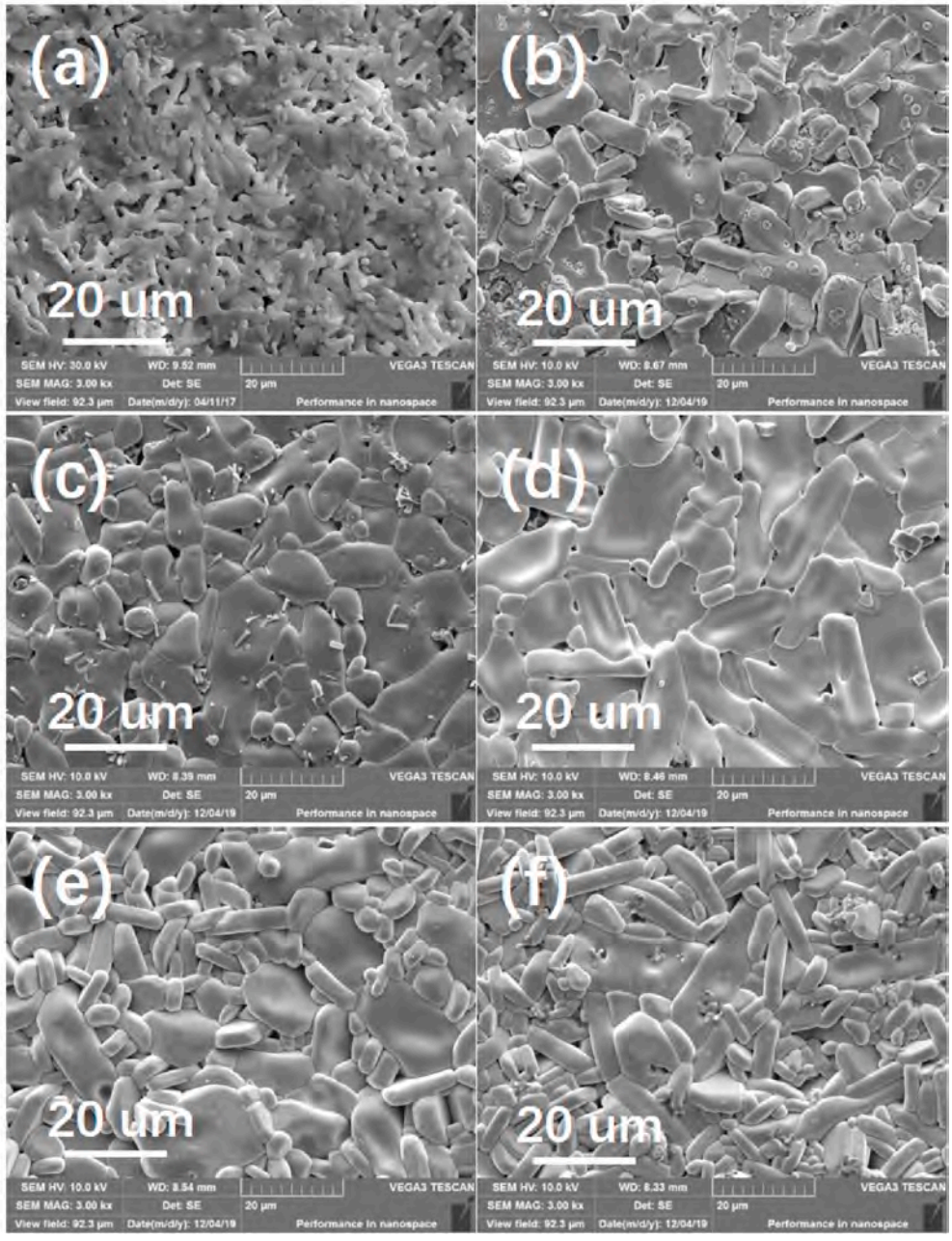

Fig. 11. Surface SEM images of (a) $Al_2Mo_3O_{12}$ sintered at 780 °C and $Al_2Mo_{3-x}W_xO_{12}$ solid solutions sintered at 900 °C for 6 h (b) $Al_2Mo_{2.5}W_{0.5}O_{12}$; (c) $Al_2Mo_2WO_{12}$; (d) $Al_2Mo_{1.5}W_{1.5}O_{12}$; (e) $Al_2MoW_2O_{12}$ and (f) $Al_2Mo_{0.5}W_{2.5}O_{12}$.

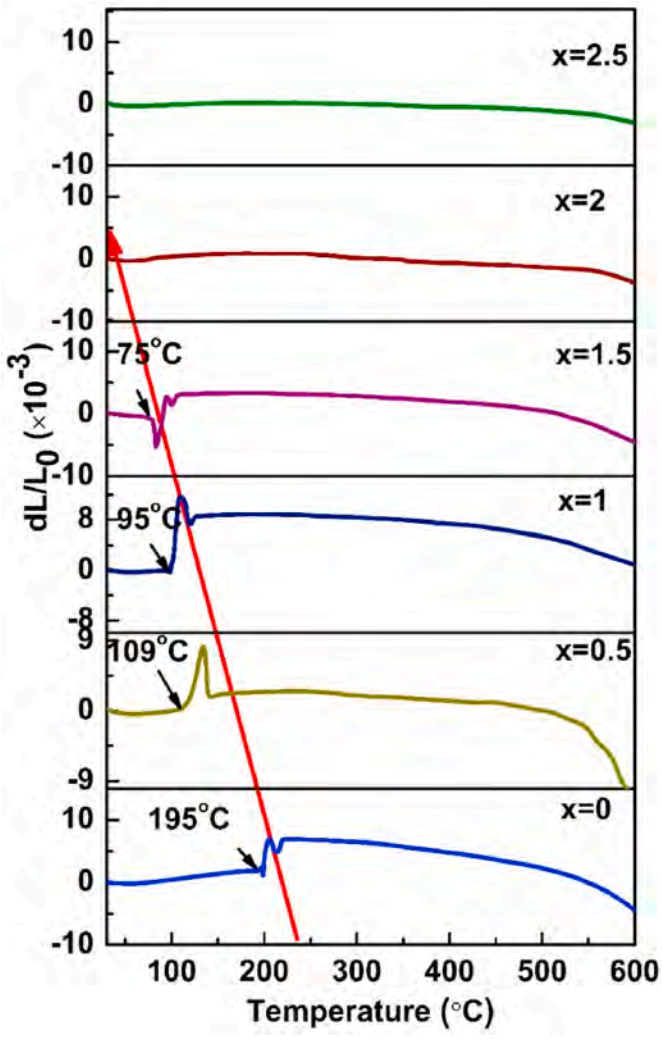

Fig. 12. Thermal expansion curves of $Al_2Mo_{3-x}W_xO_{12}$ ($0 \leq x \leq 2.5$) solid solutions.

Table 4
The CTEs of $Al_2Mo_{3-x}W_xO_{12}$ ($0 \leq x \leq 2.5$) solid solutions in the range of 30–500 °C.

Samples	CTE (× 10^{-6} °C^{-1})	Testing temperature range (°C)	CTE (× 10^{-6} °C^{-1})	Testing temperature range (°C)
$Al_2Mo_3O_{12}$	15.18	30–195	−18.06	223–500
$Al_2Mo_{2.5}W_{0.5}O_{12}$	12.26	30–109	−9.42	147–500
$Al_2Mo_2WO_{12}$	5.32	30–95	−9.53	132–500
$Al_2Mo_{1.5}W_{1.5}O_{12}$	4.56	30–75	−8.75	123–500
$Al_2MoW_2O_{12}$	/	/	−7.77	108–500
$Al_2Mo_{0.5}W_{2.5}O_{12}$	/	/	−4.25	85–500

4. Conclusions

In summary, we have successfully tuned the phase transition temperature of $Al_2Mo_3O_{12}$ to room temperature and below by single cation substitution of Sc^{3+} or W^{6+}. The crystal structure, morphology, phase transition temperature, and NTE performance dependence of the substituted cation content in $Al_2Mo_3O_{12}$ have been determined. The synthesized $Al_{1.6}Sc_{0.4}Mo_3O_{12}$ and $Al_2Mo_{0.5}W_{2.5}O_{12}$ solid solutions show stable NTE properties above room temperature. The substitution rate of A-site cation is even lower than that of B-site. This behavior could be explained by the difference in the bond strength resulting from the Al–O bond is weaker than that of the Mo–O bond in $Al_2Mo_3O_{12}$. The thermal expansion properties, which include a phase transition temperature of room temperature and below, coupled with the CTE of -2.19×10^{-6} °C^{-1} and -4.25 × 10^{-6} °C^{-1} from 100 to 550 °C, make $Al_{1.6}Sc_{0.4}Mo_3O_{12}$ and $Al_2MoW_2O_{12}$ solid solutions promising for practical application in many fields.

Declaration of competing interest

The authors declare that they have no known competing financial interests or personal relationships that could have appeared to influence the work reported in this paper.

Acknowledgement

Authors would like to acknowledge the support from the National Natural Science Foundation of China (No.51602280and No.51102207), Qing Lan Project of Jiangsu Province, Yangzhou University Science and Technique Innovation Foundation (No.2019CXJ010).

References

[1] T.A. Mary, J.S.O. Evans, T. Vogt, A.W. Sleight, Negative thermal expansion from 0.3-1050 kelvin in ZrW_2O_8, Science 272 (1996) 90–92.
[2] J.S.O. Evans, Z. Hu, J.D. Jorgensen, D.N. Argyriou, S. Short, A.W. Sleight, Compressibility, phase transitions and oxygen migration in zirconium tungstate ZrW_2O_8, Science 275 (1997) 61–65.
[3] C.A. Perottoni, J.A.H. Jornada, Pressure-induce amorphization and negative thermal expansion in ZrW_2O_8, Science 280 (1998) 886–889.
[4] G. Ernst, C. Broholm, G.R. Kowach, A.P. Ramirez, Phonon density of states and negative thermal expansion in ZrW_2O_8, Nature 396 (1998) 147–149.
[5] J.S.O. Evans, Negative thermal expansion materials, Chem. Soc. Dalton. Trans. 19 (1999) 3317–3326.
[6] S. Sumithra, A.M. Umarji, Role of crystal structure in the bulk thermal expansion of $Ln_2W_3O_{12}$ (Ln= La, Nd, Dy, Y, Er, Yb), Solid State Sci. 6 (2014) 1313–1319.
[7] M. Maczkaa, K. Hermanowicza, J. Hanuzaa, Phase transition and vibrational properties of $A_2(BO_4)_3$ compounds (A=Sc, In; B=Mo, W), J. Mol. Struct. 744–747 (2005) 283–288.
[8] T.A. Mary, A.W. Sleight, Bulk thermal expansion for tungstate and molybdates of the type $A_2M_3O_{12}$, J. Mater. Res. 14 (1999) 912–915.
[9] S. Sumithra, A.M. Umarji, Negative thermal expansion in rare earth molybdates, Solid State Sci. 8 (2006) 1453–1458.
[10] T.M. Varga, J.L. Moats, S.V. Ushakov, A. Navrotsky, Thermochemistry of $A_2M_3O_{12}$ negative thermal expansion materials, J. Mater. Res. 22 (2007) 2512–2521.
[11] M.M. Wu, J. Peng, Y.Z. Cheng, et al., Structural and controllable thermal expansion properties of $Sc_{2-x}Al_xMo_3O_{12}$, J. Alloys Compd. 577 (2013) 295–298.
[12] A.R. Soares, P.I. Pontón, L. Mancic, J.D. Almeida, C.P. Romao, M.A. White, B. A. Marinkovic, Samenvatting $Al_2Mo_3O_{12}$/polyethylene composites with reduced coefficient of thermal expansion, J. Mater. Sci. 49 (2014) 7870–7882.
[13] J.Q. Ren, K. Bi, X.L. Fu, et al., Novel $Al_2Mo_3O_{12}$-based temperature-stable microwave dielectric ceramics for LTCC applications, J. Mater. Chem. 6 (2018) 11465–11470.
[14] J.R. Ren, K. Bi, X.L. Fu, et al., Novel Bi_2O_3-added $Al_2Mo_3O_{12}$ composite microwave dielectric ceramics for ULTCC applications, J. Alloys Compd. (2020), https://doi.org/10.1016/j.jallcom.2020.153867.
[15] A.W. Sleigh, L.H. Brixner, A new ferroelastic transition in some $A_2(MO_4)_3$ molybdates and tungstates, J. Solid State Chem. 7 (1973) 172–174.
[16] A.K. Tyagi, S.N. Achary, M.D. Mathews, Phase transition and negative thermal expansion in $A_2Mo_3O_{12}$ system (A=Fe^{3+}, Cr^{3+} and Al^{3+}), J. Alloys Compd. 339 (2002) 207–210.
[17] M. Ari, P.M. Jardim, B.A. Marinkovic, et al., Thermal expansion of $Cr_{2x}Fe_{2-2x}Mo_3O_{12}$, $Al_{2x}Fe_{2-2x}Mo_3O_{12}$ and $Al_{2x}Cr_{2-2x}Mo_3O_{12}$ solid solutions, J. Solid State Chem. 181 (2008) 1472–1479.
[18] H.F. Liu, W.K. Sun, Z.P. Zhang, X.Y. Zhang, Y.X. Zhou, J. Zhu, X.H. Zeng, Tailored phase transition temperature and negative thermal expansion of Sc-substituted $Al_2Mo_3O_{12}$ synthesized by a co-precipitation method, Inorg. Chem. Front. 6 (2019) 1842–1850.
[19] R. Truitt, I. Hermes, A. Main, et al., Low temperature synthesis and characterization of $AlScMo_3O_{12}$, Materials 8 (2015) 700–716.
[20] T. Sugimoto, Y. Aoki, E. Niwa, et al., Thermal expansion and phase transition behavior of $Al_{2-x}M_x(WO_4)_3$ (M=Y, Ga, Sc) ceramics, J. Ceram. Soc. Jpn. 115 (2007) 176–181.
[21] Z.P. Zhang, Y.N. Wang, W.K. Sun, X.Y. Zhang, H.F. Liu, X.B. Chen, X.H. Zeng, Phase transition temperature and negative thermal expansion of Sc-substituted $In_2Mo_3O_{12}$ ceramics, J. Mater. Sci. 55 (2020) 5730–5740.
[22] F. Zhang, Y. Lei, Z.P. Zhang, H.F. Liu, X.Y. Zhang, X.B. Chen, X.H. Zeng, Negative thermal expansion coefficient of Sc-doped indium tungstate ceramics synthesized by co-precipitation, Ceram. Int. 46 (2020) 7259–7267.

[23] M.M. Wu, J. Peng, S.B. Han, et al., Phase transition and negative thermal expansion properties of $Sc_{2-x}Cr_xMo_3O_{12}$, Ceram. Int. 38 (2012) 6525–6529.
[24] M.M. Wu, X.Z. Liu, D.F. Chen, et al., Structure, phase transition, and controllable thermal expansion behaviors of $Sc_{2-x}Fe_xMo_3O_{12}$, Inorg. Chem. 53 (2014) 9206–9212.
[25] A. Surjith, N.K. James, R. Ratheesh, Synthesis, structural and microwave dielectric properties of $Al_2W_{3-x}Mo_xO_{12}$(x=0-3) ceramics, J. Alloys Compd. 509 (2011) 9992–9995.
[26] B. Schulz, H.L. Andersen, O.K.A. Bahri, B. Johannessen, J.N. Liu, S. Primig, N. Sharma, Electrochemical performance and structure of $Al_2W_{3-x}Mo_xO_{12}$, CrystEngComm 20 (10) (2018) 1352–1360.
[27] N. Imanaka, M. Hiraiwa, G. Adachi, H. Dabkowska, A. Dabkowski, Thermal contraction behavior in $Al_2(WO_4)_3$ single crystal, J. Cryst. Growth 220 (2000) 176–179.